A Bioluminescent Activity Dependent (BLADe) Platform for Converting Neuronal Activity to Photoreceptor Activation

Emmanuel L. Crespo[1,2]†, Akash Pal[1,3]†, Mansi Prakash[1], Alexander D. Silvagnoli[1,3], Zohair Zaidi[4], Manuel Gomez-Ramirez[5], Maya O. Tree[1], Nathan C. Shaner[6], Diane Lipscombe[5,7], Christopher Moore[5,7]*, Ute Hochgeschwender[1-3]*

1 College of Medicine, Central Michigan University, Mount Pleasant, MI 48859, USA

2 Biochemistry, Cell and Molecular Biology Graduate Program, Central Michigan University, Mount Pleasant, MI 48859, USA

3 Program in Neuroscience, Central Michigan University, Mount Pleasant, MI 48859, USA

4 Duke University, Undergraduate Neuroscience Program, Durham, NC 27710

5 Department of Neuroscience, Brown University, Providence, RI 02912, USA

6 University of California, San Diego, School of Medicine, Department of Neuroscience, 9500 Gilman Drive La Jolla, CA 92093-0662, USA

7 Carney Institute for Brain Science, Brown University, Providence, RI 02906, USA

†These authors contributed equally to this work: Emmanuel L. Crespo and Akash Pal

*Corresponding authors: Ute Hochgeschwender (hochg1u@cmich.edu) and Christopher I. Moore (Christopher_moore@brown.edu)

Abstract

We developed a platform that utilizes a calcium-dependent luciferase to convert neuronal activity into activation of light sensing domains within the same cell. The platform is based on a *Gaussia* luciferase variant with high light emission split by calmodulin-M13 sequences that depends on influx of calcium ions (Ca^{2+}) for functional reconstitution. In the presence of its luciferin, coelenterazine (CTZ), Ca^{2+} influx results in light emission that drives activation of photoreceptors, including optogenetic channels and LOV domains. Critical features of the converter luciferase are light emission low enough to not activate photoreceptors under baseline condition and high enough to activate photosensing elements in the presence of Ca^{2+} and luciferin. We demonstrate performance of this activity-dependent sensor and integrator for changing membrane potential and driving transcription in individual and populations of neurons *in vitro* and *in vivo*.

Introduction

Bioluminescence, or biolight, the emission of light generated when a luciferase enzyme oxidizes a small molecule luciferin, served as a non-invasive approach for in vitro and in vivo imaging for decades. What transforms bioluminescence from a mere imaging reagent to a versatile tool for controlling molecular processes is its combination with light sensing elements. Nature provides us with a plethora of light

sensing tools, including – but not limited to – channelrhodopsins and transcription factors[1,2]. We and others have combined luciferases with channelrhodopsins and pumps for biolight driven changes in membrane potential[3–5] as well as in reporter gene expression and intracellular localization[6–8].

As a luciferase is a genetically encoded light emitter, it can be split and made dependent on intra- and extracellular molecules, generating a palette of bioluminescent sensors, including for calcium, cyclic dinucleotides, and neurotransmitters[9]. As described above for intact luciferases, any bioluminescent sensor can, in principle, be transformed from a sensor into an actuator by using its light emission to activate photoreceptors. This opens a general platform for converting biochemical signals within and between cells into photoreceptor activation and resulting downstream changes in cellular function.

By inserting a calcium sensing moiety into a split luciferase and thus making light emission dependent on intracellular calcium levels, in neurons light emission will directly reflect the cell's activity state. This neuronal activity dependent light emission in turn can be harnessed to control photoreceptors, generating a platform for converting neural activity into real-time changes in cellular processes such as control of membrane potential for real time feedback of neuronal activity or transcription for 'read-and-write' applications. We describe critical features of this genetically encoded BioLuminescent Activity Dependence (BLADe) platform and demonstrate its performance in neurons in vitro and in vivo.

Results

Engineering of the *Gaussia* luciferase based Ca^{2+} sensor LMC4

The *Gaussia* luciferase variant sbGLuc is an efficient transmitter of photons/energy to opsin chromophores when tethered to opsins in luminopsins[4,10]. To make it Ca^{2+} dependent we split sbGLuc as was done previously for wildtype GLuc between Q88 and G89[11] and introduced the Ca^{2+} sensing moiety CaM-M13, employing the M13 sequence from the Ca2+ sensor YC3.6[12] and the calmodulin sequence from GCaMP6f[13] (**Fig. 1**). We called this split sbGLuc based Ca^{2+} indicator Lumicampsin or LMC, and LMC4 as this was the fourth split sbGLuc construct we generated[14–16].

To test for bioluminescence in response to increase in cellular Ca2+ we expressed LMC4 in HEK293 cells and imaged light emission in the presence of CTZ before and after addition of ionomycin (**Fig. 2**). There was a robust increase in light emission after Ca2+ influx into the cells. We next measured the change in bioluminescence in HEK293 cells expressing LMC4 in response to ionomycin under varying extracellular Ca2+ concentrations, ranging from 0.4875 µM to 39 µM (**Fig. 2**). LMC reported ionomycin induced Ca2+ influx/efflux at all extracellular Ca2+ conditions. The decrease in bioluminescent signal at lower extracellular Ca2+ conditions (0.4785µM -1µM) reflects the loss of intracellular Ca2+ as ionomycin moves Ca2+ from high (intracellular) to low (extracellular) concentrations. We compared the response to 39 µM extracellular Ca2+ between HEK293 cells expressing LMC4 or GCaMP6f. Under the same conditions, LMC4 reported a 43% change in signal from baseline whereas GCaMP6f reported an 8.2% change, indicating a high dynamic range for LMC4 (**Fig. 2**). Lastly, we assessed the kinetic response of LMC4 after application of CTZ and Ca2+ induction. Kinetic luminometer readings were carried out with HeLa cells expressing LMC4 or the NanoLuc based Ca2+ sensor GeNL[17], recording photon emission at baseline and after injection of CTZ (LMC4) or hCTZ (GeNL) and histamine for stimulation of intracellular Ca2+ release (**Fig. 2**). While the light emission of GeNL is higher than that of LMC4, the critical difference between the two bioluminescent

Ca2+ sensors is the low background of LMC4 in the presence of just CTZ. As the goal for our Ca2+ sensor is to not only allow visualization of Ca2+ fluctuations in the cell, but also to enable activation of light sensing actuators, this unique feature of LMC4 makes this construct suitable as an integrator of Ca2+ fluctuations with downstream effects mediated by activation of photoreceptors. Having identified a Ca2+ sensor with background luminescence below the threshold required for photoreceptor activation, and for Ca2+ specific signals emitting light sufficient for its activation, opens the possibility of a molecular integrator that directly translates neuron activation into light emission and broad based applications for modulating any cellular processes that can be effected by optogenetic tools, including changes in membrane potential or transcription.

In addition to LMC4 that contains the calmodulin sequence from GCaMP6f we generated LMCs 5-8 with calmodulin sequences from GCaMP6s and GCaMP6m[13], and from Ca2+-NL and Ca2+-eNL[17], respectively. **Supplementary Figure 2A** shows the amino acid differences between these variants. Constructs were transfected into HeLa cells, incubated with 5 µM CTZ, and the bioluminescent response to histamine induced intracellular Ca2+ release was measured in a plate reader. When measured using different emission filters across the light spectrum, all variants showed peak emission at 490 nm (**Fig. S2B**). The percent change in light emission in the presence of CTZ before and after addition of histamine averaged 156%, ranging from 132% to 188% (**Fig. S2C**). Overall, there was no significant difference between the variants and thus we proceeded with LMC4.

We made four versions of LMC4 that localize the protein to different intracellular regions by adding different localizing sequences (**Fig. S3A**). As one of the intended uses of LMC4 is to activate nearby channelrhodopsins, we compared two ways of localizing the Ca2+ dependent light emitter to the inner cell membrane, by adding a C-terminal farnesylation (LMC4f) or an N-terminal myristoylation (myLMC4) signal. We compared Ca2+ induced light emission of the two constructs in HeLa cells and found the farnesylated version to perform significantly better (**Fig. S3B**). We compared LMC4f to LMC4er that localizes to the ER via a C-terminal KDEL sequence. HEK293 cells expressing either construct were tested in the absence (0 µM) or presence (39 µM) of extracellular Ca2+ and 10 µM CTZ. Acute Ca2+ flux was elicited by addition of 2 µM ionomycin. In the absence of extracellular Ca2+ the signal from LMC4er expressing cells was higher than that from LMC4f expressing cells due to ER mobilization of internal Ca2+ stores. In contrast, in 39 µM extracellular Ca2+ a high bioluminescence signal was observed in LMC4f expressing HEK cells with very low signal from LMC4er expressing cells (**Fig. S3C**). Lastly, we generated miLMC4 that targets the Ca2+ sensor to mitochondrial membranes. Mitochondria localization was confirmed by co-expressing miLMC4 with a mitochondrial tag BacMam2.0-Mito-GFP in HeLa cells. Confocal images show that the Mito-GFP tag and miLMC4 co-localize (**Fig. S3D**).

LMC4 reports Ca^{2+} flux *in vitro* and *in vivo*

To test LMC4's efficiency in reporting Ca2+ fluctuations from cells in culture, we transfected primary cardiomyocytes with the LMC4f plasmid and imaged cultures on DIV 4 with an EMCCD camera. Cells were incubated with 100 µM CTZ for ~10 minutes before imaging started. 10 µM ATP was added around 14.53 seconds, after which the contractility of the cells increased. ROI analysis showed high activity peaks starting around the 50 second mark (**Fig. 3A**). For in vivo imaging of hearts Swiss Webster mice were transduced with AAV2/9 CAG LMC4f virus and imaged using an IVIS Lumina LT In Vivo Imaging System 3 weeks later. Prior to imaging the animals received an intraperitoneal injection of 100 µg of water soluble

CTZ. ROI analysis shows that it took 10 minutes after ip injection for the bioluminescent signal from the heart to reach its peak which was maintained for 15 minutes before slowly returning to baseline an hour after ip injection (**Fig. 3B**).

We next tested LMC4 reporting of Ca2+ flux in the brain *in vivo*. Mouse barrel cortex was transduced with AAV2/9 hSyn LMC4f virus and the area was imaged through a cranial window in head fixed mice. During continuous imaging, CTZ (50 µL) was injected through the lateral ventricle, followed by direct cortical injection of NMDA (1 µL) 5 minutes later. Comparison of bioluminescence emission over the transduced versus un-transduced area shows no change from baseline emission between the two areas with CTZ application alone, but a substantial increase in emission from neurons transduced with LMC4f shortly after NMDA-induced neural activity (**Fig. 4A**). We further compared bioluminescence emission from areas transduced with the Ca2+-dependent LMC4f versus an intact, non-Ca2+-dependent luciferase, GLuc. Normalized light emission traces diverge only over the area expressing LMC4f and only after an increase in neural activity following NMDA injection (**Fig. 4B**).

LMC4 integrates Ca2+ influx with change in transcription in cell lines *in vitro*

Given the low background luminescence of LMC4 in the presence of just the luciferin and the robust light emission upon Ca2+ influx we assessed the possibility of using LMC4 to integrate Ca2+ influx with modulating cellular processes that can be effected by optogenetic tools. Co-expressing LMC4 with a light sensing transcription factor would translate Ca2+ dependent light emission into transcription of a co-transformed reporter gene.

To test this, we employed the light sensing transcription factor EL222[18]. Under exposure to blue light, EL222 dimerizes and then binds to its promoter 5 x C120, leading to transcription of the reporter gene (**Fig. 5A**). We wanted to see whether bioluminescence emitted from LMC4 in the presence of Ca2+ and CTZ would lead to transcription of a reporter firefly luciferase, FLuc. HEK293 cells were co-transfected with LMC4, EL222, and the EL222 dependent FLuc reporter construct. Exposure of cells to both CTZ and Ca2+ through ionomycin induced influx resulted in substantial increase in reporter transcription in a luciferin concentration-dependent manner, with larger -fold increase with higher concentration of luciferin (200 µM versus 100 µM final concentration) (**Fig. 5B**). Background transcription in the presence of CTZ alone or with neither CTZ nor Ionomycin-induced Ca2+ influx is negligible. We also tested bioluminescent driven transcription in HeLa cells, where addition of histamine leads to release of Ca2+ from intracellular stores. HeLa cells were co-transfected with LMC4 or without a luciferase, and EL222 and the EL222 dependent FLuc reporter construct. Reporter gene expression was assessed after plates were left in the dark, received CTZ for 1 minute, or received CTZ for 1 minute plus histamine. Again, transcription of the reporter is only seen in the presence of both CTZ and Ca2+ (**Fig. 5C**).

LMC4 integrates neural activity with change in membrane potential in neurons in vitro

As Ca2+ influx is a proxy for neural activity, we assessed the possibility of using LMC4 to integrate neural activity with modulating cellular processes that can be effected by optogenetic tools. Co-expressing LMC4 with channelrhodopsins would translate Ca2+ dependent light emission into excitation or inhibition of the neuron depending on the biophysical properties of the co-expressed opsin (**Fig. 6A**).

We first tested this in individual whole cell patched neurons under current injection. We generated I/O curves from rat embryonic primary cortical neurons expressing LMC4f together with an inhibitory opsin, hGtACR2[19], an excitatory opsin, ChR2(C128S)[20], or without an opsin. In neurons expressing an inhibitory opsin together with the integrator LMC4, increasing current injection results in a right-shift of the I/O curve in the presence of CTZ due to bioluminescence activation of the opsin and hyperpolarization of the cell (**Fig. 6B**). In contrast, co-expression of LMC4 with an excitatory opsin leads to a left-shift of the I/O curve due to bioluminescence activation of the opsin and additional depolarization of the cell (**Fig. 6C**). Increasing current injections result in increasing firing rates with identical I/O curves in the presence or absence of CTZ/bioluminescence when no opsin is expressed (**Fig. 5D**) or in the absence of CTZ/bioluminescence (**Fig. 6E**).

We then tested the efficacy of this real-time self-regulation of neural activity in neural populations plated on multi electrode arrays. Populations were transduced with AAV delivering the inhibitory opsin hGtARC2 or the excitatory opsin ChR2(C128S), alone or together with LMC4f. Addition of CTZ to firing neurons resulted in decrease of spiking when LMC4 was co-transduced with the inhibitory opsin (**Fig. 7A, B**), and in increased spiking with the excitatory opsin (**Fig. 7C, D**). These effects of CTZ were not observed when opsins were expressed by themselves.

LMC4 converts neural activity into photoreceptor activation *in vivo*

Ultimately, the value of this activity dependent bioluminescent platform is in its applicability to in vivo experiments. To test LMC4's efficacy to drive transcription in neurons in vivo, we injected mixtures of AAV9-hSyn-LMC4-P2A-dTomato, AAV9-CAG-EL222, and AAV9-5xC120-EYFP into the prefrontal cortex of mice. Once expression reached maximum levels, mice received injections intraventricularly of either NMDA and vehicle, CTZ alone, or CTZ and NMDA, reflecting increase of activity of neurons with vehicle instead of luciferin (vehicle + NMDA), luciferin exposure to neurons without increased activity (CTZ), and increase of activity of neurons in the presence of luciferin (CTZ + NMDA). Evaluation of EL222 dependent expression of the EYFP reporter showed a significant increase in EYFP expression in the presence of both NMDA and CTZ, demonstrating activity dependent transcription in real time (**Fig. 8**).

There currently is no tool that enables all molecular self-regulation of neural activity by harnessing real-time changes in intracellular dynamics, such as fluctuations in intracellular calcium. Building on our *in vitro* and *in vivo* observations, we next wanted to determine if LMC4 can integrate changes to neural activity via physiological sensory inputs to cell-autonomously alter network dynamics *in vivo*. We injected Cre-dependent versions of LMC4 and the excitatory opsin CheRiff[21] into the left cortex of Emx1-Cre mice to target both constructs to excitatory pyramidal neurons within vibrissa SI (vSI). We performed laminar silicon probe recordings in vSI of anesthetized mice (**Fig 9A**), constantly perfusing either ACSF or ACSF containing CTZ and simultaneously presenting vibrissal deflections (**Fig 9B**).

By expressing CheRiff in vSI pyramidal neurons, we predicted increased multi-unit activity with either external LED light source or through LMC4 bioluminescence driven opsin activation in the presence of the luciferin. To investigate the spontaneous spiking behavior in the presence of CTZ, constant bath application of vehicle or CTZ was performed. Perfusion of CTZ lead to enhanced multiunit activity as compared to the vehicle epochs (**Fig 9C**, Wilcoxon signed rank test $p=2.32 \times 10^{-10}$, $p < 0.05$ with post hoc Bonferroni correction for multiple comparison, vehicle epoch: M= 26.4, SD= 16.61, median= 22.1, range= 5.4-80.4,

CTZ epoch: M= 52.7, SD= 26.0, median= 43.6, range= 17.5-126.6). Therefore, LMC4 can enhance spontaneous cortical neural activity through the photoactivation of light-sensitive cation channels in vivo through bioluminescent mediated optogenetics. Optogenetic stimulation was carried out at the end of every recording session. An 8Hz sinusoidal stimulation pattern was applied for 500ms in LMC4 and CheRiff expressing mice to elicit recruitment of opsin expressing neurons. Upon LED stimulation we observed robust optogenetic enhancement in multi-unit activity (8Hz, 500ms, **Fig 9D inset**). Responsive channels were observed during the 500ms stimulation window relative to the baseline window (**Fig 9D**, Kruskal-Wallis test $p= 3.23 \times 10^{-08}$; $p < 0.05$ with post hoc Bonferroni correction for multiple comparison, during baseline: M= 24.13 Hz, SD= 8.51, median= 22.7, range: 14.4-54.8, during stimulation: M= 83.1 Hz, SD= 96.63, median= 45.2, range=16.9-406.83). In contrast, non-responsive channels had no change in multi-unit activity during LED stim (**Fig 9D,** Kruskal-Wallis test $p > 0.05$, during baseline: M=40.5, SD= 32.4, median= 22.7, range=0.1-173.26, during stimulation: 0.1-173.07). The observed enhancement of via LED or CTZ stimulation suggest that the LMC4f/CheRiff expressing neuron activity changes are mediated through bioluminescence mediated optogenetic activation of CheRiff as a novel approach for activating opsins via self-generated calcium dependent light-emission.

Our above *in vivo* extracellular electrophysiology experiments demonstrated LMC4's ability to alter neocortical dynamics through presumably spontaneous changes in intracellular calcium. We next sought to assess if LMC4 mediated activity dependent enhancement of neural dynamics can be driven through vibrissae sensory recruitment of LMC4/Cheriff expressing neurons. To this end, we tested for predictive relationships between enhanced neural activity as a function of vibrissae stimulus amplitude by comparing the multiunit activity during the vehicle and CTZ epochs. Following sensory stimulation, typical responses of multi-unit activity can be observed within vSI ~10-20ms following low amplitude vibrissae stimulation (**Fig 9E**). There is an increase in multi-unit activity in sensory responsive sites in low stimulus trials in the presence of CTZ compared to vehicle (blue vs grey, trace **Fig 9E,** low stimulation amplitude group).

We systematically randomized the vibrissae stimulation amplitude during the vehicle and CTZ epochs. In order to isolate BLADe optogenetic recruitment of cortical activity, we compared 0-50 ms poststimulus window responses during the vehicle and CTZ epochs. A single vibrissae deflection terminates within 25 ms poststimulus while the next deflection occurs 50 ms postimulus. We directly compared sensory evoked multiunit activity during the 0-25ms (early phase) and 26-50ms (late-phase) windows to determine both real-time and delayed enhancement of neural activity, respectively. There is an enhancement during trials from the same recorded sites with CTZ versus vehicle perfusion epochs, with increasing sensory evoked responses during both the early (**Fig 9F**, Kruskal-Wallis test, low: $p= 7.62 \times 10^{-06}$, mid: $p= 1.9 \times 10^{-06}$, max: $p= 3.72 \times 10^{-09}$, $p < 0.05$ with post hoc Bonferroni correction for multiple comparison) and late (**Fig 9G,** Kruskal-Wallis test, low: $p= 7.63 \times 10^{-06}$, mid: $p= 3.81 \times 10^{-06}$, max: $p= 2.61 \times 10^{-08}$, $p < 0.05$ with post hoc Bonferroni correction for multiple comparison) poststimulus phases. Collectively, this demonstrates that LMC4 can convert spontaneous activity and sensory evoked changes into activity dependent control of neocortical network dynamics.

Discussion

Tremendous innovation is currently being applied to placing cellular processes under control of light, including channel opening and transcription. Bioluminescence is evolving as a highly advantageous mechanism for driving these light dependent processes. This luciferase-luciferin approach is a highly

biocompatible mechanism that can be aligned to photosensing receivers on the molecular scale and provides a photonic report of its activation timing. The genetically encoded light emitter can be targeted to specific cell populations and can be arranged inside or outside of cells and across cells. Further, bioluminescent light output can be made dependent on intra- and extracellular molecules, enabling exciting new directions for the control of cellular dynamics. The 'light switch' is a small molecule luciferin and thus light activation is determined by the experimenter, and its temporal and spatial kinetics are dependent on route of application and concentration of the luciferin.

By using the concept of a luciferase split by a sensing moiety, any bioluminescent sensor can be made into an actuator by combining it with a photoreceptor. Here we selected as an example for proof-of-concept experiments and to demonstrate the versatility of the approach a calcium dependent luciferase in combination with channelrhodopsins and a transcription factor. By using a *Gaussia* luciferase variant, LMC4, we identified critical features needed for this bioluminescent Ca2+ sensor to work as a neural activity dependent driver of photosensing molecules, mainly the need for light emission in the presence of luciferin and low Ca2+ levels to be below the activation threshold of photoreceptor chromophores and with increased Ca2+ levels emit enough light for photoreceptor activation. We successfully applied this prototype Ca2+ dependent luciferase, LMC4, for converting neural activity into changes in membrane potential and into transcription of a reporter gene in cells in vitro and in vivo.

The neural control of behavior is crucially dependent on rapid dynamical processes, from the biophysical cycle driving action potentials to those creating the timing and duration of spike trains. Understanding specific dynamics in behavior requires allowing them to take their normal course, only manipulating the system when it shows the dynamic of interest. Reflecting its utility, this kind of control theory approach is increasingly being implemented to test how brain dynamics impact behavior. Typically, this approach uses electrodes to detect macro-scale events (e.g., a sleep Spindle oscillation) with external algorithms. This detection then triggers an invasive perturbation such as electrical stimulation to impact this event (e.g., extend its duration, and ask the impact on memory)[22,23]. These studies provide unique insights but require substantial hardware - either multiple implanted recording electrodes or large windows or fiber implants to obtain calcium triggers, computer intermediaries to host algorithms, and fibers or stimulating electrodes to deliver responses.

The BL-ADe platform provides an entirely new approach to dynamic control, detecting calcium increases to drive feedback through local opsins with cellular precision. By providing real-time, sub-cellular feedback control, driving opsins only when a cell is active, it is a unique way to sense such dynamics and locally and immediately alter their trajectory within a single neuron. As shown in Figure 9, this control mechanism can enhance behaviorally relevant neural activity patterns (e.g., sensory responses), but only when the cells are activated above a threshold. This method can allow triggering based on underlying dynamics in specific cell types in specific foci, for example, briefly increasing the firing of only those pyramidal neurons that burst, to test if their increased firing duration enhanced sensory detection. This approach is also ideal for directly targeting dynamical processes. As an example, using BL-ADe to trigger enhanced hyperpolarization (or, depolarization) only after individual neurons show a large calcium event is ideal for altering the operative mechanism to extend or suppress macro-scale phenomena. Extensive prior study has shown that opsin recruitment by bioluminescence light does not 'leak' to other nearby neurons unless specifically designed to achieve 'Interluminescence' (please see Prakash et al., 2022[24] for further discussion). As such, this new dynamical control strategy is inherently cell-specific (and, could be leveraged to be sub-cellular in precision with targeted expression, e.g., to soma or axons).

Another challenging current question in neuroscience is how to identify and study the whole ensemble of active neurons that appears to meet the representational needs of a specific behavior: Which cells in which contexts form the necessary chain of actors that selectively lead to specific perceptions, actions and cognition. A recent generation of approaches was created that attempts to advance this essential area of study by using calcium sensitivity as the mechanism that creates activation-dependence, and timed light to target specific behavioral epochs. The leading examples of this approach are Cal-Light[25] and FLARE[26]. In essence, the coincidence of light and neural activity results in release of a transcription factor: light application leads a LOV domain to exposure a protease cleavage site; the protease will only be in proximity to the cleavage site in the presence of high Ca^{2+}, with photostimulation providing a high degree of temporal and spatial control. This Ca2+ dependent protease strategy has significant limitations in that it requires a highly complicated molecular design, increasing the potential for failure points in distinct cell types. More importantly, light pulses from a fiber optic are required to drive expression, which does not allow whole ensemble tagging.

To better meet the need, we and others have been developing bioluminescence as the source for light controlled, activity dependent transcription. The LuCID approach is a recent advance in this domain[27] that uses the design logic we are advancing here, i.e. using a Ca2+ dependent luciferase to activate a light sensing transcription system. Different from our design, dependence for light emission on Ca2+ is not regulated by conformational change within the luciferase; rather, free-floating luciferase components (NanoBit system) are reconstituted by a Ca2+ dependent process, enabling blue-light dependent dimerization of the FKF1/GI transcription system. While not yet (to our knowledge) tested in vivo, this approach shows powerful increases in selective transcription in reduced systems and begins to resolve the limitations of Cal-Light and FLARE. The LuCID system's re-combination of free luciferase 'bits' shows minutes time scale sensory specificity, and its reliance on diffusion makes fast (e.g., single action potential burst) kinetics impossible to achieve. Our new calcium indicator uses a simple split-luciferase design, greatly enabling further tuning to research needs. Importantly, any new innovations in Ca2+ sensor designs can be implemented in better performing BLADe tools. For example, the new CaBLAM sensor (Lambert BX) is a single molecule that already shows sub-second onset precision, aligning its activity scales with the intensity of neural activation[28].

Our data show proof-of-principle of a highly versatile Bioluminescent Activity Dependent (BLADe) Platform for converting neuronal activity to photoreceptor activation that can be improved by engineering Ca2+ dependent luciferases with higher light emission and improved kinetics as well as different dynamic ranges for Ca2+ sensing. Further, this platform can be extended to neural activity dependent control of the many other optogenetic tools for subcellular applications in neuroscience and to applications using other intra- and extracellular molecules triggering luciferase reconstitution and light emission.

REFERENCES

1. Rost, B. R., Schneider-Warme, F., Schmitz, D. & Hegemann, P. Optogenetic Tools for Subcellular Applications in Neuroscience. *Neuron* **96**, 572–603 (2017).

2. Losi, A., Gardner, K. H. & Moglich, A. Blue-Light Receptors for Optogenetics. *Chem. Rev.* **118**, 10659–10709 (2018).

3. Berglund, K., Birkner, E., Augustine, G. J. & Hochgeschwender, U. Light-Emitting

Channelrhodopsins for Combined Optogenetic and Chemical-Genetic Control of Neurons. *PLoS One* **8**, e59759 (2013).

4. Berglund, K. *et al.* Luminopsins integrate opto- and chemogenetics by using physical and biological light sources for opsin activation. *Proc. Natl. Acad. Sci. U. S. A.* **113**, E358–E367 (2016).

5. Tung, J. K., Gutekunst, C.-A. & Gross, R. E. Inhibitory luminopsins: genetically-encoded bioluminescent opsins for versatile, scalable, and hardware-independent optogenetic inhibition. *Sci. Rep.* **5**, 14366 (2015).

6. Crespo, E. L., Bjorefeldt, A., Prakash, M. & Hochgeschwender, U. Bioluminescent Optogenetics 2.0: Harnessing Bioluminescence to Activate Photosensory Proteins In Vitro and In Vivo. *J. Vis. Exp.* (2021) doi:10.3791/62850.

7. Li, T. *et al.* A synthetic BRET-based optogenetic device for pulsatile transgene expression enabling glucose homeostasis in mice. *Nat. Commun.* **12**, (2021).

8. Parag-Sharma, K. *et al.* Engineered BRET-Based Biologic Light Sources Enable Spatiotemporal Control over Diverse Optogenetic Systems. *ACS Synth. Biol.* (2020) doi:10.1021/acssynbio.9b00277.

9. Petersen, E. D. *et al.* Bioluminescent Genetically Encoded Glutamate Indicator for Molecular Imaging of Neuronal Activity. *bioRxiv* 2021.06.16.448690 (2022) doi:10.1101/2021.06.16.448690.

10. Welsh, J. P., Patel, K. G., Manthiram, K. & Swartz, J. R. Multiply mutated Gaussia luciferases provide prolonged and intense bioluminescence. *Biochem. Biophys. Res. Commun.* **389**, 563–8 (2009).

11. Kim, S. B., Sato, M. & Tao, H. Split Gaussia luciferase-based bioluminescence template for tracing protein dynamics in living cells. *Anal. Chem.* **81**, 67–74 (2009).

12. Saito, K. *et al.* Luminescent proteins for high-speed single-cell and whole-body imaging. *Nat. Commun.* **3**, 1262 (2012).

13. Chen, T.-W. *et al.* Ultrasensitive fluorescent proteins for imaging neuronal activity. *Nature* **499**, 295–300 (2013).

14. Pal, A. *et al.* Split Gaussia luciferase based genetically encoded calcium indicator. in *Society for Neuroscience Abstracts* 92.07 (2016).

15. Pal, A. *et al.* Characterization, sub-cellular targeting and novel applications of a split Gaussia luciferase based genetically encoded calcium indicator. in *Society for Neuroscience Abstracts* 717.12 (2017).

16. Pal, A. *et al.* A multifunctional bioluminescent calcium indicator. in *Society for Neuroscience Abstracts* No. 612.16. (2018).

17. Suzuki, K. *et al.* Five colour variants of bright luminescent protein for real-time multicolour bioimaging. *Nat. Commun.* **7**, 13718 (2016).

18. Motta-Mena, L. B. *et al.* An optogenetic gene expression system with rapid activation and deactivation kinetics. *Nat. Chem. Biol.* (2014) doi:10.1038/nchembio.1430.

19. Govorunova, E. G., Sineshchekov, O. A., Janz, R., Liu, X. & Spudich, J. L. Natural light-gated anion

channels: A family of microbial rhodopsins for advanced optogenetics. *Science (80-.).* science.aaa7484- (2015) doi:10.1126/science.aaa7484.

20. Berndt, A., Yizhar, O., Gunaydin, L. A., Hegemann, P. & Deisseroth, K. Bi-stable neural state switches. *Nat. Neurosci.* **12**, 229–34 (2009).

21. Hochbaum, D. R. *et al.* All-optical electrophysiology in mammalian neurons using engineered microbial rhodopsins. *Nat. Methods* **11**, 825–833 (2014).

22. Novitskaya, Y., Sara, S. J., Logothetis, N. K. & Eschenko, O. Ripple-triggered stimulation of the locus coeruleus during post-learning sleep disrupts ripple/spindle coupling and impairs memory consolidation. *Learn. Mem.* **23**, 238–248 (2016).

23. Lustenberger, C. *et al.* Feedback-Controlled Transcranial Alternating Current Stimulation Reveals a Functional Role of Sleep Spindles in Motor Memory Consolidation. *Curr. Biol.* **26**, 2127–2136 (2016).

24. Prakash, M. *et al.* Selective control of synaptically-connected circuit elements by all-optical synapses. *Commun. Biol.* **5**, 33 (2022).

25. Lee, D., Hyun, J. H., Jung, K., Hannan, P. & Kwon, H.-B. A calcium- and light-gated switch to induce gene expression in activated neurons. *Nat. Biotechnol.* **35**, 858–863 (2017).

26. Wang, W. *et al.* A light- and calcium-gated transcription factor for imaging and manipulating activated neurons. *Nat. Biotechnol.* **35**, 864–871 (2017).

27. Erdenee, E. & Ting, A. Y. A Dual-Purpose Real-Time Indicator and Transcriptional Integrator for Calcium Detection in Living Cells. *ACS Synth. Biol.* **11**, 1086–1095 (2022).

28. Lambert, G.G., Crespo E.L., *et al*. CaBLAM: a high-contrast bioluminescent calcium indicator derived from an engineered Oplophorus gracilirostris luciferase. *bioRxiv* (2023).

29. Pacak, C. A. *et al.* Recombinant adeno-associated virus serotype 9 leads to preferential cardiac transduction in vivo. *Circ. Res.* **99**, (2006).

30. Gomez-Ramirez, M., More, A. I., Friedman, N. G., Hochgeschwender, U. & Moore, C. I. The BioLuminescent-OptoGenetic in vivo response to coelenterazine is proportional, sensitive, and specific in neocortex. *J. Neurosci. Res.* **98**, 471–480 (2020).

31. Prakash, M., Medendorp, W. E. & Hochgeschwender, U. Defining parameters of specificity for bioluminescent optogenetic activation of neurons using in vitro multi electrode arrays (MEA). *J. Neurosci. Res.* (2018) doi:10.1002/jnr.24313.

MATERIALS AND METHODS

Chemicals

Coelenterazine (CTZ) for in vitro (#303) and in vivo (#3031) experiments was purchased from Nanolight Technologies. The Calcium Calibration Buffer Kit #1 from Life Technologies was used to prepare Zero Ca^{2+} buffer and 39 µM Ca^{2+} buffer. All other chemicals, including Ionomycin and Histamine, were purchased from Sigma.

Plasmids

A pcDNA3.1 backbone with the CMV promoter was used to insert gBlocks (IDT) that encode for N-sbGluc, CaM-M13 variants, C-sbGluc and p2a dTomato by Gibson cloning (New England Biolabs HiFi DNA Master Mix). Coding sequences from plasmids for GCaMP6f, hGtACR2, and ChR2(C128S) (see Supplementary Table) were cloned into the pcDNA3.1-CMV backbone. For viral vectors, coding sequences were cloned into a pAAV vector downstream of a CAG or hSyn promoter, or into a pAAV-EfIa-DIO construct.

Plasmid	Source	Reference
pcDNA3.1-CMV-LMC4-P2A-dTomato		this paper
pcDNA3.1-CMV-LMC5-P2A-dTomato		
pcDNA3.1-CMV-LMC6-P2A-dTomato		
pcDNA3.1-CMV-LMC7-P2A-dTomato		
pcDNA3.1-CMV-LMC8-P2A-dTomato		
pcDNA3.1-CMV-LMC4f-P2A-dTomato		
pcDNA3.1-CMV-myLMC4-P2A-dTomato		
pcDNA3.1-CMV-LMC4er-P2A-dTomato		
pcDNA3.1-CMV-miLMC4-P2A-dTomato		
pAAV-hSyn-LMC4f-P2A-dTomato		
pAAV-CAG- VP-EL222		
pAAV-5xC120-EYFP		
pAAV-EfIa-DIO-CheRiff-EYFP		
pAAV-EfIa-DIO-LMC4f-P2A -dTomato		
pcDNA3.1-5xC120-EYFP		
pcDNA3.1-CAG-VP-EL222	Kevin Gardner, CUNY	18
pcDNA3.1-5xC120-FireflyLuc	Kevin Gardner, CUNY	18
pcDNA3-CMV-GeNL(Ca2+)_520	Addgene plasmid # 85204	17
pAAV.Syn.GCaMP6f.WPRE.SV40	Addgene plasmid # 10083	13
pFUGW-hGtACR2-EYFP	Addgene plasmid # 67877	19
pLenti-CaMKIIa-hChR2(C128A)-EYFP-WPRE	Addgene plasmid # 20293	20
pAAV-hsyn-CheRiff-eGFP	Addgene plasmid #51697	21

pcDNA3.1-CAG-VP-EL222 and pcDNA3.1-5xC120-FireflyLuc were kindly provided by Dr. Kevin Gardner, CUNY, New York, NY

pAAV.Syn.GCaMP6f.WPRE.SV40 was a gift from Douglas Kim & GENIE Project (Addgene plasmid # 100837 ; http://n2t.net/addgene:100837 ; RRID:Addgene_100837)

GeNL(Ca2+)_520/pcDNA3 was a gift from Takeharu Nagai (Addgene plasmid # 85204 ; http://n2t.net/addgene:85204 ; RRID:Addgene_85204)

pLenti-CaMKIIa-hChR2(C128S)-EYFP-WPRE was a gift from Karl Deisseroth (Addgene plasmid # 20294 ; http://n2t.net/addgene:20294 ; RRID:Addgene_20294)

pFUGW-hGtACR2-EYFP was a gift from John Spudich (Addgene plasmid # 67877 ; http://n2t.net/addgene:67877 ; RRID:Addgene_67877)

pAAV-hSyn-CheRiff-eGFP was a gift from Adam Cohen (Addgene plasmid # 51697 ; http://n2t.net/addgene:51697 ; RRID:Addgene_51697)

AAV

AAV2/9 preparations were generated by triple lipofection of HEK293-FT cells and harvesting viral particles as previously described[4].

Animals

All experiments involving animals were carried out following the guidelines and protocols approved by the Institutional Animal Care and Use Committee at the participating universities and were in compliance with the US National Research Council's Guide for the Care and Use of Laboratory Animals, the US Public Health Service's Policy on Humane Care and Use of Laboratory Animals, and Guide for the Care and Use of Laboratory Animals.

Mice were group-housed in ventilated cages under 12-hour reverse light cycle, provided with tap water and standard chow and allowed to feed ad libitum.

C57/BL6 (JAX #000664), Emx1-Cre (JAX# 005628), and Swiss Webster (Charles River) mice of both sexes were used.

Cell Culture and Cell Transformation

HEK293 and HeLa cells were obtained from ATCC (American Type Culture Collection), expanded, and aliquots at low passage numbers were frozen. Cells were grown in Gibco DMEM media supplemented with 10% Fetal Bovine Serum, 1% Glutamax, 0.5 % Pen-Sterp, 1% Non-Essential Amino Acids and 1% sodium pyruvate. Cells were cultured at 37°C and 5% atmospheric carbon dioxide. Cells were transfected with Lipofectamine 2000 or 3000 in accordance with the manufacturer's instructions.

Primary E18 rat hippocampal neurons were prepared from tissue shipped from BrainBits (Transnetyx) following the vendor's protocol. Neurons were grown in Gibco Neurobasal Media supplemented with 2% B27 supplement and 0.1% gentamycin and 1% Glutamax. Neurons were nucleofected with plasmids of interest using the Lonza 2b Nucleofector and Rat Neuron Nucleofector Kit (Lonza, VPG-1003) according to the manufacturer's instruction, then seeded. Or neurons were nucleofected, seeded, then transduced with AAV the next day. Neurons were seeded on PDL-coated glass coverslip (Neuvitro) in 12-well tissue culture plates (1 x 10^5 neurons per well) or were plated on the electrode area of 1-well MEA dishes (60MEA200/30iR-Ti; Multi Channel Systems, Germany) coated with PEI (0.1%) and laminin (50µg/ml) (1x10^5 neurons/10 µL/well) as described in detail in Prakash 2020.

Primary cardiomyocytes were harvested from E18 Swiss Webster mice, papain digested and plated on 35mm glass bottom dishes (MatTek) for real time bioluminescence imaging. Primary cardiomyocytes were grown in Claycomb Media supplemented with 10% HL-1 screened FBS, 100µg/mL penicillin/streptomycin, 0.1mM norepinephrine and 2% Glutamax. Cells were nucleofected with plasmids of interest using the Lonza 2b Nucleofector and Rat cardiomyocyte Nucleofector Kit (Lonza, VAPE-1002) according to the manufacturer's instruction.

Microscopy

Initially, all transfected cells were imaged using a Zeiss Axio Observer A1 microscope with a LD A-Plan 20x/0 air objective and a Hamamatsu Orca Flash 4.0 CMOS camera to confirm expression by fluorescence microscopy at 50ms exposure except for LMCer, which was imaged at a 10 seconds exposure.

Confirmation of subcellular localization and imaging of brain sections were done on an Olympus Fluoview 300 CLSM confocal microscope with a 60x/1.3 Oil objective.

Bioluminescence Imaging

In vitro

For photon counting HEK293 and HeLa cells were seeded on Costar 96 well clear bottom white plates and luminescence was measured in a SpectraMax® L luminometer (Molecular DevicesTM).

For real-time bioluminescence imaging we used a Zeiss Axio Observer A1 microscope with a Fluar 40x/1.3 Oil objective with either a Hamamatsu Orca Flash 4.0 CMOS camera or an Andor iXon Ultra 888 EM-CCD camera with their respective softwares. HEK293 and HeLa cells were imaged in imaging solution (CaCl2 1.25mM, HEPES 19.7mM, KCl 4.7mM, KH2PO4 1.2mM, MgSO4 1mM, NaCl 130mM, dextrose 0.5, pH 7.2-7.4) with either 100µM or 12.5 µM CTZ. Primary cardiomyocytes were imaged in Tyrode's solution (NaCl 137mM, KCl 2.7mM, MgCl2 1mM, CaCl2 1.8mM, Na2HPO4 0.2mM, NaHCO3 12mM, D-glucose 5.5mM, pH 7.2-7.4) supplemented with 10µM norepinephrine and 100 µM CTZ.

In vivo

Heart: P0 Swiss Webster mice were anesthetized on ice and 1µl of AAV2/9 CAG LMC4f virus (~$1x10^{13}$ vg/mL) was diluted in 49µL HBSS and injected through the superficial temporal vein using a 28½ gauge needle. We chose AAV2/9 for these experiments because it has preferential expression in cardiac tissue[29]. Animals were imaged 3.5 months post viral injection in IVIS Lumina LT In Vivo Imaging System (PerkinElmer, Waltham, MA) with Living Image 4.5.2 software (RRID:SCR_014247). On the day of imaging, animals were injected intraperitoneally with 100 µg of water soluble CTZ (in a volume of 250uL) right before imaging for 60 minutes with an exposure time of 1 second.

Brain: AAV2/9-hSyn-LMC4f-P2A-dTomato (450 nl) was injected across three locations in left primary somatosensory (SI) cortex (150 nl per site) as described in detail in Gomez-Ramirez 2020[30]. Water-soluble CTZ (Nanolight Technology #3031) was diluted to yield a concentration of 2.36 mM. CTZ and NMDA injections were done directly in cortex. Bioluminescence was measured using an electron multiplier charge coupled device (EMCCD) camera (Ixon 888, Andor) attached to a Navitar Zoom 6000 lens system (Navitar, 0.5× lens). Images were collected in a custom-made light-tight chamber with an exposure time of 10 s, and the EM gain set to 30. Imaging data were recorded using the Solis image acquisition and analysis software (Solis 4.29, Andor).

Electrophysiology recordings from primary neurons

Neurons were nucleofected with LMC4f alone or co-nucleofected with either an inhibitory opsin, hGtACR2, or an excitatory opsin, ChR2(C128S). Post nucleofection, neurons were plated on laminin-coated glass coverslips (15mm, Neuvitro) in culture medium consisting of Neurobasal Medium (Gibco # 21103-049), B-27 supplement (Gibco # 17504-044), 2 mM Glutamax (Gibco # 35050-061), and 5% Fetal Calf Serum (FCS). The following day, the medium was replaced with serum-free medium (NB-Plain medium). Half of the medium was replaced with fresh NB-Plain medium every 3–4 days thereafter. Neurons were

used for whole cell patch clamp recordings between DIVs 21–25. For patch clamp recording, a coverslip was transferred to a recording chamber mounted on an upright microscope (BX51WI, Olympus) and perfused with aCSF containing (in mM): 121 NaCl, 2.8 KCl, 1 NaH_2PO_4, 26 $NaHCO_3$, 2 $CaCl_2$, 2 $MgCl_2$ and 15 D-glucose (310 mOsm/kg, pH 7.3-7.4) at a rate of 1.5 ml/min. All solutions were bubbled with a gas mixture of 95% O_2 and 5% CO_2. Whole-cell patch clamp recordings were performed using a Multiclamp 700b amplifier and Digidata 1440 digitizer together with the pClamp recording software (Molecular Devices). Borosilicate glass micropipettes were manufactured using a PC-100 puller (Narishige) and had resistances of 3–5 MΩ. In current clamp recordings, pipettes were filled with intracellular solution containing (in mM): 130 K-gluconate, 10 KCl, 15 HEPES, 5 Na_2-phosphocreatine, 4 Mg-ATP and 0.3 Na-GTP (310 mOsm/kg, pH 7.3). The aCSF was supplemented with D-AP5 (50 µM), CNQX (15 µM) and picrotoxin (100 µM) to block fast glutamatergic and GABAergic synaptic transmission. Rs was compensated using bridge balance. Firing frequencies were calculated from the total number of action potentials produced per unit time during depolarizing current injections (10 sweeps, 1.5 sec duration) in episodic stimulation acquisition mode, at a membrane potential of -70mV, before and after CTZ (100 µM) or vehicle treatments.

MEA Recordings

Once the neurons were matured (DIV14-DIV19), only those were included in the analysis that were consistently spiking and were positive for expression of their respective opsins as tested by shining blue LED light (470nm) on the culture and recording increase or decrease of spiking. Total recording time was 900 seconds. MEAs were subjected to 10µM CTZ at around 600 seconds. Experimental cultures expressed both LMC4f and an opsin (ChR2(C128S) or hGtARC2), while control MEAs only expressed the opsin. MC Rack software was used for data acquisition. All MEA analysis was done offline with MC Rack software (MultiChannel Systems; RRID:SCR_014955) and NeuroExplorer (RRID:SCR_001818) as described in detail in Prakash et al., 2018[31].

Transcription in vivo

Mixtures of AAV9 preparations of the 3 constructs (pAAV-hSyn-LMC4f-P2A-dTomato, pAAV-CAG-VP-EL222, pAAV-5xC120-EYFP) were stereotaxically injected into the medial prefrontal cortex of mice. Three or more weeks later mice received injections of NMDA alone, CTZ alone, or CTZ and NMDA. Brains were collected 18 hours later and sections imaged under a confocal microscope. Images were evaluated for EYFP cell density per area by an individual blind to the animal identifier and counts were graphed.

Electrophysiology in vivo

Mixtures of AAV9 preparations of 2 constructs (pAAV-EFIa-DIO-LMC4f-P2A-dTomato, pAAV-EfIa-DIO-CheRiff-EYFP) were stereotaxically injected into the barrel cortex of Emx1-Cre mice. Two or three weeks later, a cranial window (~1mm) over the barrel cortex was created in preparation for acute extracellular recordings. Mice were fitted with a custom metal headpost and secured in place to allow perfusion tubing to be positioned next to the craniotomy, allowing for constant aCSF inflow (for bioluminescence CTZ was diluted to 50 µM in aCSF). All macrovibrissae on the right side of the mouse were secured ~3mm from the mystacial pad. A custom-made clamp was glued to a piezoelectric bender (Noliac CMBP09), positioned to move all macrovibrissae in the caudorostral direction, with a half-sine wave velocity profile with a rising phase (6ms) and a slower relaxation phase (20ms). On each trial, 20Hz vibratory vibrissal stimulus trains (10 deflections, 500ms) were delivered for 1000 trials total. On a trial by trial and randomized basis, the stimulus amplitude varied between 0 to maximal amplitude (~1mm deflection). For each recording

session, aCSF was constantly perfused for the first 500 trials and CTZ was then perfused for the remaining 500 trials.

All recordings in barrel cortex were conducted under light isoflurane anesthesia. Laminar probes consisted of single shank,32-channel silicon probes with a fiber optic 50µm above the highest recording site (A1x32 Poly2-5mm-50s-177-OA32LP, Neuronexus Technologies; 0.15mm silver wire reference). Data was sampled at 30kHz and passed through a digital amplifier (Cereplex-µ, Blackrock Microsystems), and directed through HDMI to the Cereplex Direct data acquisition box (Blackrock Microsystems).

Spikes were extracted and classified using Kilosort. Manual curation of single unit was conducted using Phy by assessing the cross-correlograms and auto-correlograms. Units were then identified as either regular spiking or fast-spiking based on trough-to-peak (RS if > 0.4 ms, FS if <0.4ms). Sensory responsive units were defined by their stimulus probability as the area under the receiver operating curve (AUROC) in an ideal observer analysis, where the ideal observer discriminated maximal stimulus amplitude trials from zero amplitude trials based on the firing rates in the first 20ms period stimulus onset. Significance was determined by 99% confidence intervals of the stimulus probability, constructed by bootstrapping 1000 times. Peristimulus time histograms (PSTH) were obtained by averaging spike times across trials by constructing matrices with 1ms bin resolution timestamps, multiplying by 1000 to obtain units in Hz, and smoothing with a Gaussian kernel (kernel window size of 20ms and SD of 3ms).

Statistics

All analysis was carried out using MATLAB and SPSS software. Data are displayed as mean±standard error of the mean (SEM). We ran two-way repeated measures and One-way ANOVA. Tukey's post hoc was run where significant main effect was found.

Electrophysiological in vivo data was high pass filtered at 250Hz to extract spikes. Spike data was thresholded at -63µV and sorted for each channel based on waveform characteristics using Principal Components Analysis (PCA). Spikes were binned to calculate frequency of firing over time. Differences between groups were assessed using two-way repeated measures ANOVAs (repeat trials per mouse). For ex vivo electrophysiological data, statistical significance between groups was determined using Student's T-test.

Acknowledgments

We would like to thank all members of Bioluminescence Hub (http://www.bioluminescencehub.org/) laboratories for their feedback, discussions, and thoughtful comments throughout the progression of this work.

Competing interests

The authors have no conflicts of interest to declare.

Author contributions

Conceptualization, AP, ELC, NCS, CIM, UH; Validation, AP, ELC, CIM, NCS, UH; Formal Analysis, AP, ELC; Investigation, AP, ELC, MP, ADS, ZZ, MG-R, MOT; Data Curation, AP, ELC; Writing—Original Draft, AP, ELC; Writing—Review & Editing, ELC, NCS, CIM, UH; Visualization, AP, ELC; Supervision, CIM, NCS, UH; Project Administration, UH; Funding Acquisition, CIM, NCS, UH.

Funding

This work was supported by National Institutes of Health grants R21MH101525 and R21EY026427, and National Science Foundation grant DBI-1707352.

FIGURE LEGENDS

Figure 1. Design of a *Gaussia* luciferase based Ca^{2+} sensor. **A**. Schematic of the Ca^{2+} dependent luciferase LMC4. sbGLuc (light blue) is split by a CaM-M13 module (purple) and thus non-functional even in the presence of its luciferin, CTZ (orange). Binding of Ca^{2+} (yellow) reconstitutes a functional luciferase and enables light emission in the presence of CTZ. **B**. Elements of the coding sequence for LMC4: *Gaussia* luciferase signal peptide (red), N- and C-terminal of sbGLuc (light blue), calmodulin sequence from GCaMP6f (purple), M13 sequence (purple), and various linker regions (gray). **C**. Ribbon diagrams of GLuc indicating 9 alpha helices. Left: Of the 9 alpha helices α4 and α7 form the most rigid block of the luciferase stabilized by a disulphide bond between Cysteine 65 and 77. Right: The Calcium sensing moiety, CaM-M13 was inserted between Q88 and G89. In its unbound state, the CaM-M13 destabilizes the C65-C77 disuphide bond just by pushing the two halves away from each other. When bound to Ca2+, the CaM-M13 pulls on both halves and stabilize the C65-C77 disulphide bond to render the luciferase functional.

Figure 2. Features of LMC4. **A**. Bioluminescence, brightfield and fluorescent images of HEK cells expressing LMC4. Cells were continuously imaged in the presence of 12.5 µM CTZ and ionomycin was added to a final concentration of 2 µM (black arrow in graph). The different color ROIs in the bioluminescence image are traced in the graph to the right. Images were taken with an Andor iXon Ultra 888 EM-CCD camera, EM Gain 100. **B**. Percent change in bioluminescence in HEK293 cells expressing LMC4 in response to 2 µM ionomycin under varying extracellular Ca2+ concentrations. Cells were pre incubated with 5 µM CTZ and varying concentrations of Ca2+; acute Ca2+ flux was initiated by injection of ionomycin before photon counting in a luminometer. **C**. Response of LMC4 and GCaMP6f to acute Ca2+ flux. HEK293 cells expressing LMC4 or GCaMP6f were held in 39 µM extracellular Ca2+ concentration and ionomycin was added to 2µM final concentration. LMC4 expressing HEK cells were pre-incubated with CTZ at 5 µM final concentration. Bioluminescence readings for LMC4 were taken on a SpectraMax-L luminometer and fluorescent images for GCaMP6f were taken on a Zeiss AxioObserver A1 microscope with a Hamamatsu Ocra Flash4.0 CMOS camera before and after the addition of ionomycin. Graph displays percent change in signal before and after ionomycin induced Ca2+ flux. **D**. Kinetic bioluminescence readings in HeLa cells transfected with LMC4 or GeNL, showing the change in light emission with addition of luciferin (CTZ or hCTZ) and of histamine relative to the baseline readings before exposure to luciferin. The graph to the right shows the percent change in light response to histamine induced intracellulat Ca2+ release relative to the light response to just luciferin.

Figure 3: LMC4 reports Ca2+ flux in cardiomyocytes in vitro and in vivo. **A**. Primary cardiomyocytes were nucleofected with LMC4f and imaged with an Andor iXon Ultra 888 EM-CCD camera (exposure time 200 ms, sampling rate 4.01 Hz, EM gain 300, Binning 4*4) after incubating in 100 µM CTZ. 10 µM ATP was added around 14.53 seconds. Pseudocolored images for ROI analysis are shown on the left, graphic display of ROIs over time on the right. Orange and gray labeled arrows t1 – t3 indicate matching images and parts of the graph. **B**. Pseudocolored IVIS images of bioluminescence response to CTZ (100 µg ip) of a mouse expressing LMC4f in the heart. Left image corresponds to beginning and right image corresponds to peak of light emission shown in the graph to the right.

Figure 4: LMC4 reports Ca2+ flux in the brain in vivo. Mouse barrel cortex was transduced with AAV2/9 and the area was imaged through a cranial window in head fixed mice. CTZ (50 µL) was injected through the lateral ventricle, while NMDA (1 µL) was applied via direct cortical injection. **A**. Comparison of bioluminescence emission over area transduced with AAV-LMC4f (ROI 1, blue line) versus area un-

transduced (ROI 2, red line). Onset of CTZ and NMDA injection are indicated. **B**. Comparison of bioluminescence emission over area transduced with Ca2+ dependent luciferase, AAV-LMC4f (red box in image, red line in graph) versus area transduced with non-Ca2+ responsive luciferase, AAV-GLuc (blue box in image, blue line in graph). Onset of CTZ and NMDA injections are indicated.

Figure 5: LMC4 integrates Ca2+ flux with change in transcription in vitro **A**. Schematic of LMC4 leading to bioluminescence mediated dimerization of the light sensing transcription factor EL222 in the presence of Ca2+ and CTZ. The homodimer then binds to its promoter 5 x C120 and leads to transcription of the reporter gene. **B**. HEK293 cells were co-transfected with LMC4, the photosensitive transcription factor EL222, and the EL222 dependent FLuc reporter construct. Exposure of cells to bioluminescence by addition of CTZ for 1 minute together with Ionomycin to cause Ca^{2+} influx resulted in substantial increase in reporter transcription in a luciferin concentration-dependent manner. Background transcription in the presence of CTZ alone or with neither CTZ nor Ionomycin-induced Ca^{2+} influx is negligible. **C**. HeLa cells were co-transfected with LMC4 or without a luciferase, and EL222 and the EL222 dependent FLuc reporter construct. Reporter gene expression was assessed after plates were left in the dark (DARK), received CTZ for 1 minute (CTZ ONLY), or received CTZ for 1 minute plus histamine (HIST). In HeLa cells addition of histamine leads to release of Ca^{2+} from intracellular stores. Transcription of the reporter is only seen in the presence of both CTZ and Ca^{2+}.

Figure 6: LMC4 integrates neural activity with change in membrane potential in single neurons in vitro. **A**. Schematic of farnesylated LMC4 anchored at the inside of the cell membrane, close enough to a channelrhodopsin to effect light-mediated activation with the co-incidence of Ca2+ and CTZ. **B – E**. Rat embryonic primary cortical neurons were nucleofected with LMC4f together with the inhibitory opsin hGtACR2 (B), the excitatory opsin ChR2(C128S) (C, E), or alone (D). Whole-cell patch recordings were performed with current injections to generate I/O curves before and after application of coelenterazine (CTZ, B – D) or of vehicle (VEH, E). **B**. In neurons expressing an inhibitory opsin together with LMC4, increasing current injection results in a right-shift of the I/O curve in the presence of CTZ due to bioluminescence activation of the opsin and hyperpolarization of the cell. **C**. In neurons expressing an excitatory opsin together with LMC4, increasing current injection results in a left-shift of the I/O curve in the presence of CTZ due to bioluminescence activation of the opsin and additional depolarization of the cell. There is no shift in I/O curves for the controls, either when CTZ application leads to bioluminescence in neurons expressing LMC4 alone without an opsin present (**D**), or vehicle application in neurons co-expressing LMC4 with an opsin (**E**).

Figure 7: LMC4 integrates neural activity with change in membrane potential in neural populations in vitro. Rat embryonic primary cortical neurons were nucleofected with the inhibitory opsin hGtACR2 (A, B), or the excitatory opsin ChR2(C128S) (C, D) and plated on multielectrode arrays (MEAs). Half of each set of MEAs was transduced the next day with AAV9 hSyn LMC4f. Example traces from individual electrodes of the MEAs are shown to the left; graphs of electrodes combined across MEA recordings are shown on the right. **A, B**. Application of CTZ leads to decrease in firing activity when an inhibitory opsin is present (upper trace, left graph), but not if neurons only express the opsin (lower panel, right graph). **C, D**. The same is true for co-expression of LMC4f and an excitatory opsin, where CTZ application leads to increase in firing (upper trace, blue line in graph) versus no change in firing without LMC4f (lower trace, gray line in graph).

Figure 8: LMC4 converts neural activity into reporter transcription *in vivo*. **A**. Schematic of components expressed in neurons: LMC4-P2A-dTomato, EL222, and the reporter construct for EL222 dependent

transcription of EYFP. **B – E**. Mixtures of AAV9 preparations of the 3 constructs were stereotaxically injected into the medial prefrontal cortex of mice. Three or more weeks later mice received injections of NMDA alone, CTZ alone, or CTZ and NMDA. Brains were collected 18 hours later and sections imaged under a confocal microscope. Examples of images of dTomato (upper panels) and EYFP (lower panels) are shown for the three groups. While all mice express dTomato, indicating expression of LMC4, robust expression of the EYFP reporter is only visible in sections from mice that received CTZ together with NMDA induced neural stimulation (**D**). Images were evaluated for EYFP cell density per area and counts were graphed (**E**).

Figure 9: LMC4 converts neural activity into change in firing rate *in vivo*. **A**. Schematic of the experimental design. Extracellular electrophysiology recordings from SI barrel cortex during varied vibrissal deflections (zero, low, mid, max intensities) for 500ms at 20Hz. **B**. Schematic of the experimental timeline. Each recording consisted of 1000 trials (~2.5 hour sessions) where ACSF containing vehicle or CTZ was constantly perfused over the craniotomy. During each treatment epoch, vibrissal deflections were randomly presented. In the presence of the sensory stimulus and vehicle (grey box), there is no activity dependent light emission of LMC4. In contrast, in the presence of CTZ and the sensory stimulus (blue box), sensory recruitment leads to activity dependent bioluminescence and subsequently photoactivation of opsins in neurons. **C**. MUA firing rate before and after the bath application of CTZ over the craniotomy. **D.** MUA firing rate for responsive and non-responsive channel to optogenetic stimulation. *Inset:* the pattern LED signal (teal), percent change of firing rate for responsive (blue) and non-responsive channels (grey). **E.** Peristimulus time histograms from two distinct recording sites reflect changes in spiking activity evoked by contralateral sensory driven recruitment during the vehicle (grey) and CTZ (blue) treatment periods during low amplitude vibrissae stimulation. **F.** Mean multiunit activity responses to during the early phase window during the vehicle vs CTZ epoch as a function of low, medium, and max vibrissae stimulus amplitude. *Inset:* schematic of the analog signal controlling the piezo stimulator, red box is the window of time where the mean was quantified. **G.** Same as F, but during the late phase window. All data are plotted as mean +/- SEM.

Supplemental Figure S1. Amino acid sequences of sbGLuc and LMC4. **A**. aa sequence of sbGLuc with landmark mutations of sbGLuc versus wildtype GLuc color coded. **B**. aa sequence of LMC4 with landmarks indicated by colors and underlines.

Supplemental Figure S2. Different versions of Lumicampsins based on different calmodulin moieties. **A**. All LMC derivatives have the same sbGluc split between residues Q88 and G89 and the same M13 moiety with different calmodulin moieties inserted: GCaMP6f (LMC4), GCaMP6s (LMC5), GCaMP6m (LMC6), Ca2+-NL (Saito et al., 2012; LMC7), Ca2+-eNL (Suzuki et al., 2016; LMC8). Dark blue font indicates amino acids varying between the five versions. **B**. Emission wavelength of LMC variants. The different LMC constructs were transiently expressed in HeLa cells and light emission after CTZ and histamine addition was measured across the wavelength spectra using a Molecular Devices M5 plate reader. All derivatives have peak emission at 490 nm. **C**. Bioluminescence response to Ca2+ flux. Change in luminescence in the presence of CTZ in response to 10 µM Histamine in HeLa cells.

Supplemental Figure S3. Different versions of LMC4 based on different subcellular targeting sequences. **A**. Schematics of four versions of LMC4 targeting the Ca2+ sensor to the inner cell membrane via a farnesylation or myristoylation signal, to the ER via a KDEL signal, or to the mitochondrial membrane via a mitochondrial targeting signal of cytochrome c oxidase. **B**. Mean fold change of light emission from HeLa cells expressing LMC4f or myLMC4 after histamine-induced Ca2+ flux. **C**. Bioluminescence response to

ionomycin induced Ca2+ flux in HEK293 cells expressing LMC4f or LMC4er in the presence of CTZ and in the absence or presence of extracellular Ca2+. **D**. Confocal images of HeLa cells expressing miLMC4-dTomato and BacMam2.0-Mito-GFP.

Figure 1

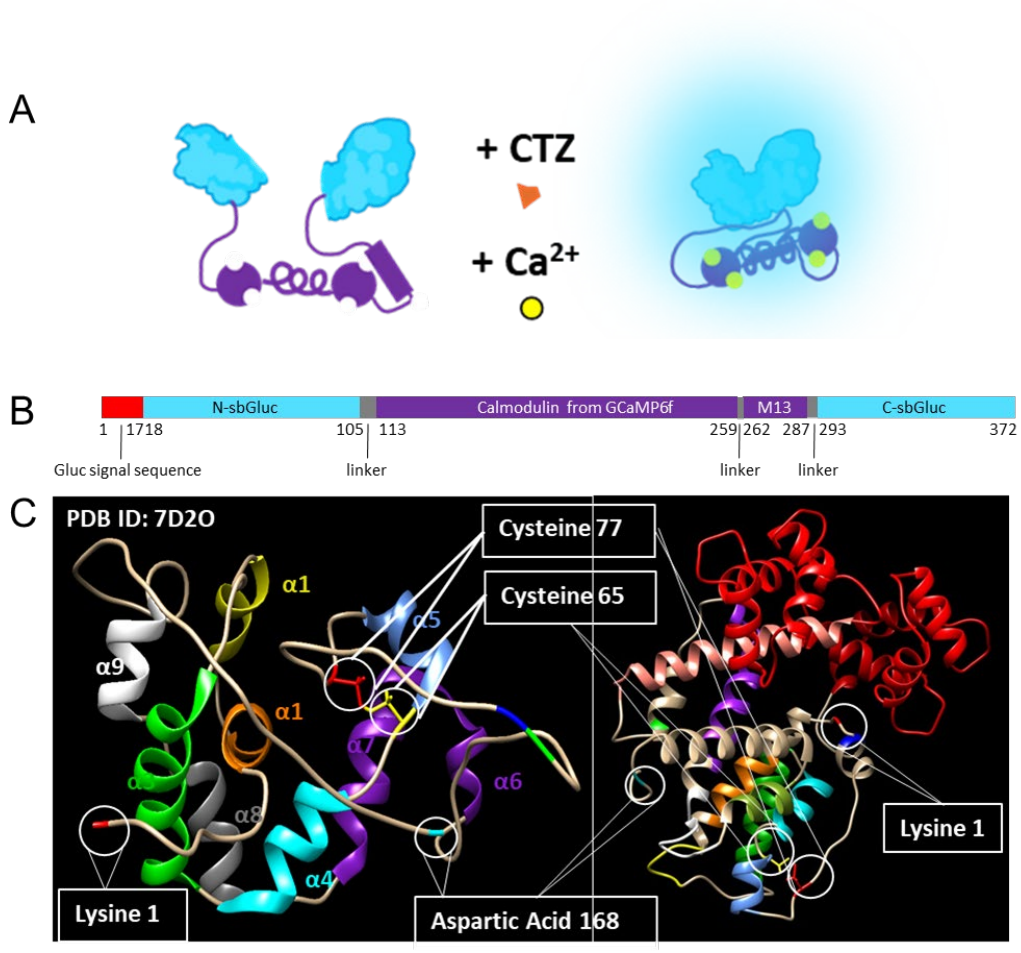
A
+ CTZ
+ Ca2+
B
N-sbGluc
Calmodulin from GCaMP6f
M13
C-sbGluc
1
1718
105
113
259
262
287
293
372
Gluc signal sequence
linker
linker
linker
C
PDB ID: 7D2O
Cysteine 77
Cysteine 65
α1
α5
α9
α1
α7
α6
α8
α4
Lysine 1
Aspartic Acid 168
Lysine 1

Figure 2

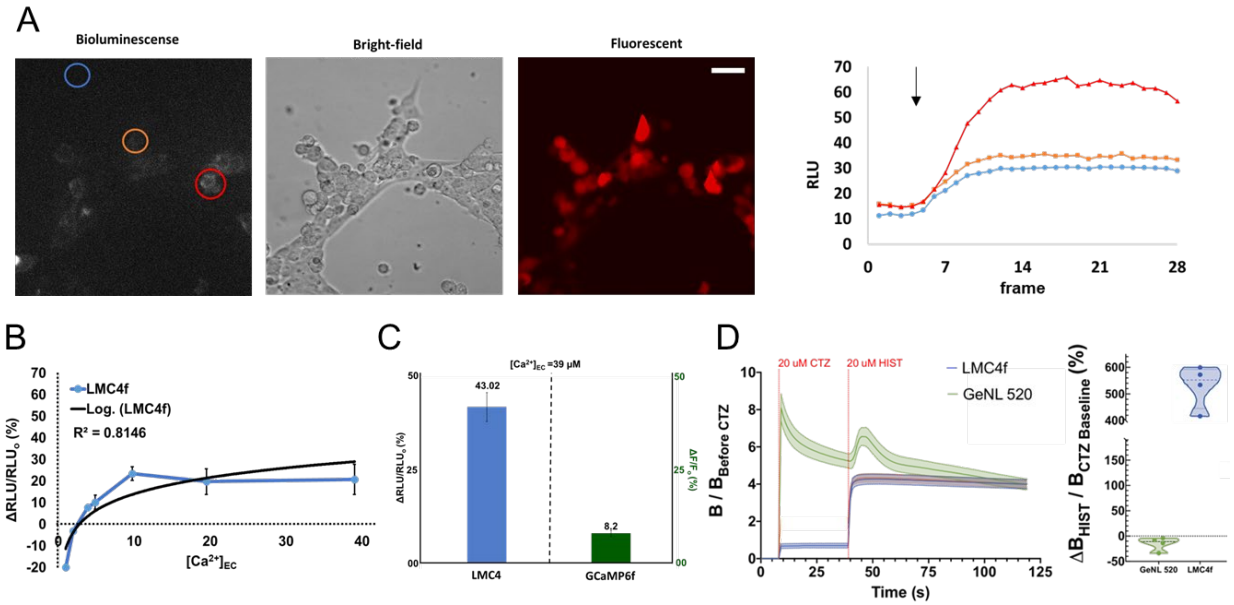
A
Bioluminescense
Bright-field
Fluorescent
RLU
frame
B
LMC4f
Log. (LMC4f)
R² = 0.8146
ΔRLU/RLU₀ (%)
[Ca²⁺]EC
C
[Ca²⁺]EC =39 µM
43.02
8,2
ΔRLU/RLU₀ (%)
ΔF/F₀ (%)
LMC4
GCaMP6f
D
20 uM CTZ
20 uM HIST
LMC4f
GeNL 520
B / BBefore CTZ
Time (s)
ΔBHIST / BCTZ Baseline (%)
GeNL 520
LMC4f

Figure 3

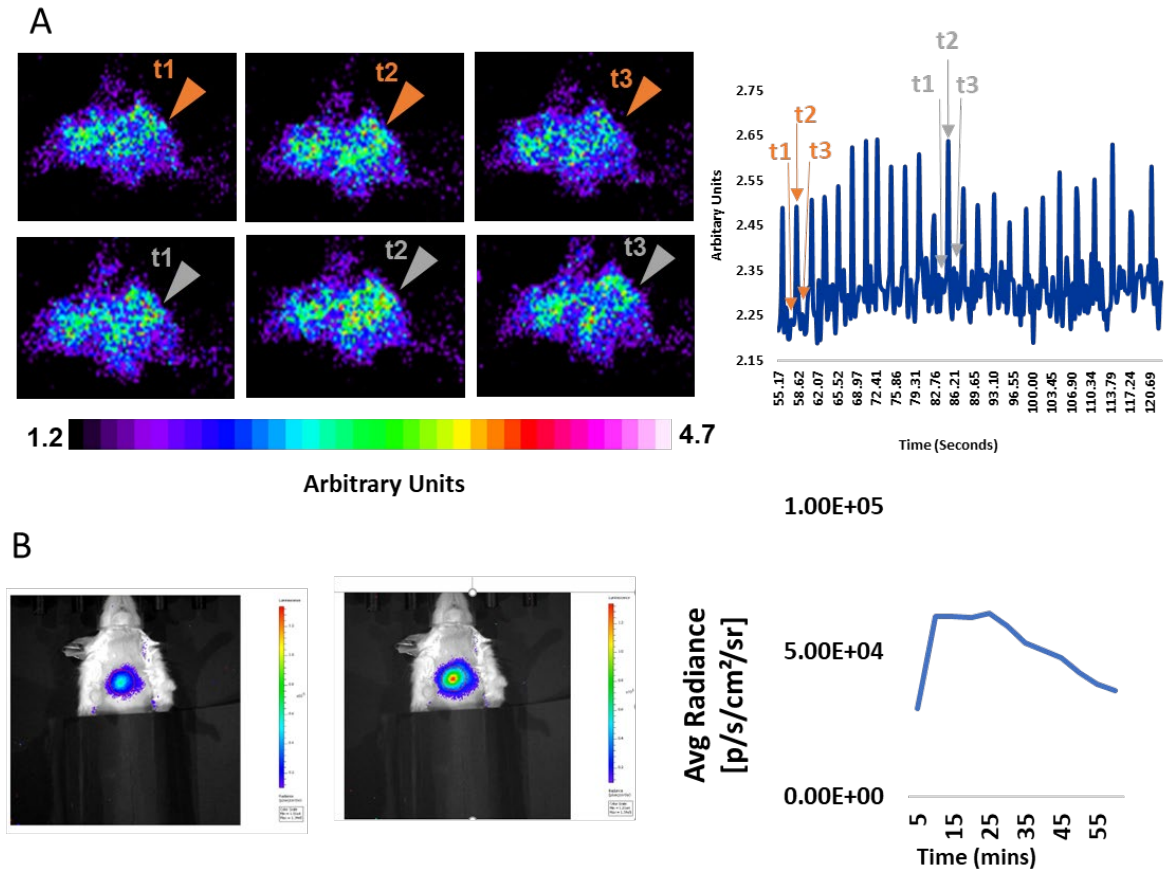
A
t1
t2
t3
t1
t2
t3
1.2
4.7
Arbitrary Units
Arbitary Units
2.75
2.65
2.55
2.45
2.35
2.25
2.15
55.17
58.62
62.07
65.52
68.97
72.41
75.86
79.31
82.76
86.21
89.65
93.10
96.55
100.00
103.45
106.90
110.34
113.79
117.24
120.69
Time (Seconds)
B
1.00E+05
5.00E+04
0.00E+00
Avg Radiance [p/s/cm²/sr]
5
15
25
35
45
55
Time (mins)

Figure 4

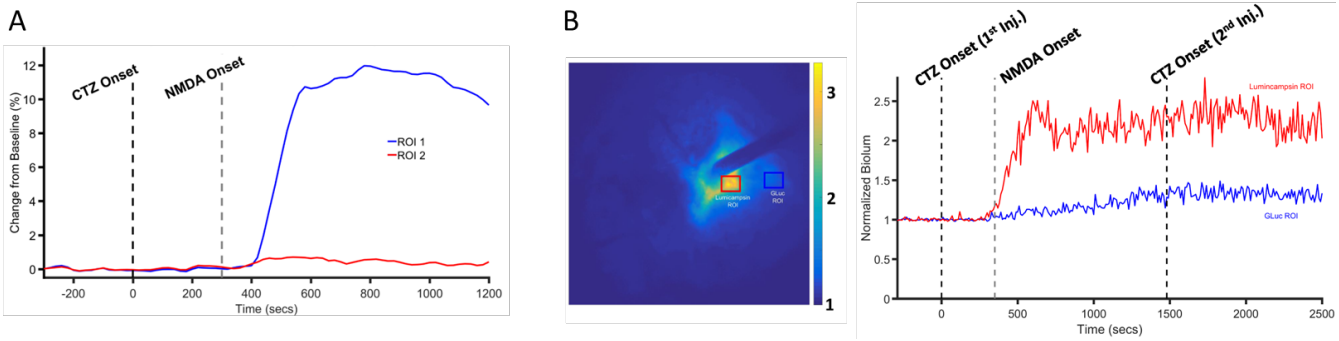
A
CTZ Onset
NMDA Onset
Change from Baseline (%)
ROI 1
ROI 2
Time (secs)
B
3
2
1
CTZ Onset (1st Inj.)
NMDA Onset
CTZ Onset (2nd Inj.)
Lumincampsin ROI
GLuc ROI
Normalized Biolum
Time (secs)

Figure 5

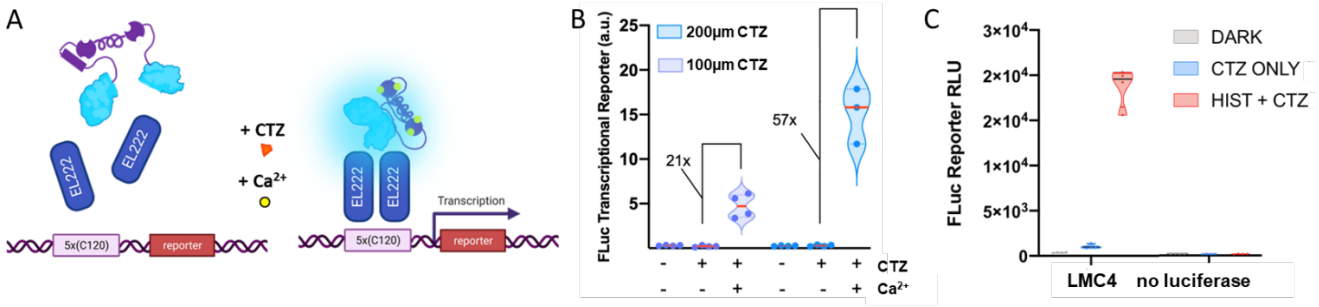
A
EL222
EL222
+ CTZ
+ Ca2+
5x(C120)
reporter
EL222
EL222
Transcription
5x(C120)
reporter
B
FLuc Transcriptional Reporter (a.u.)
200µm CTZ
100µm CTZ
21x
57x
CTZ
Ca2+
C
FLuc Reporter RLU
DARK
CTZ ONLY
HIST + CTZ
LMC4
no luciferase

Figure 6

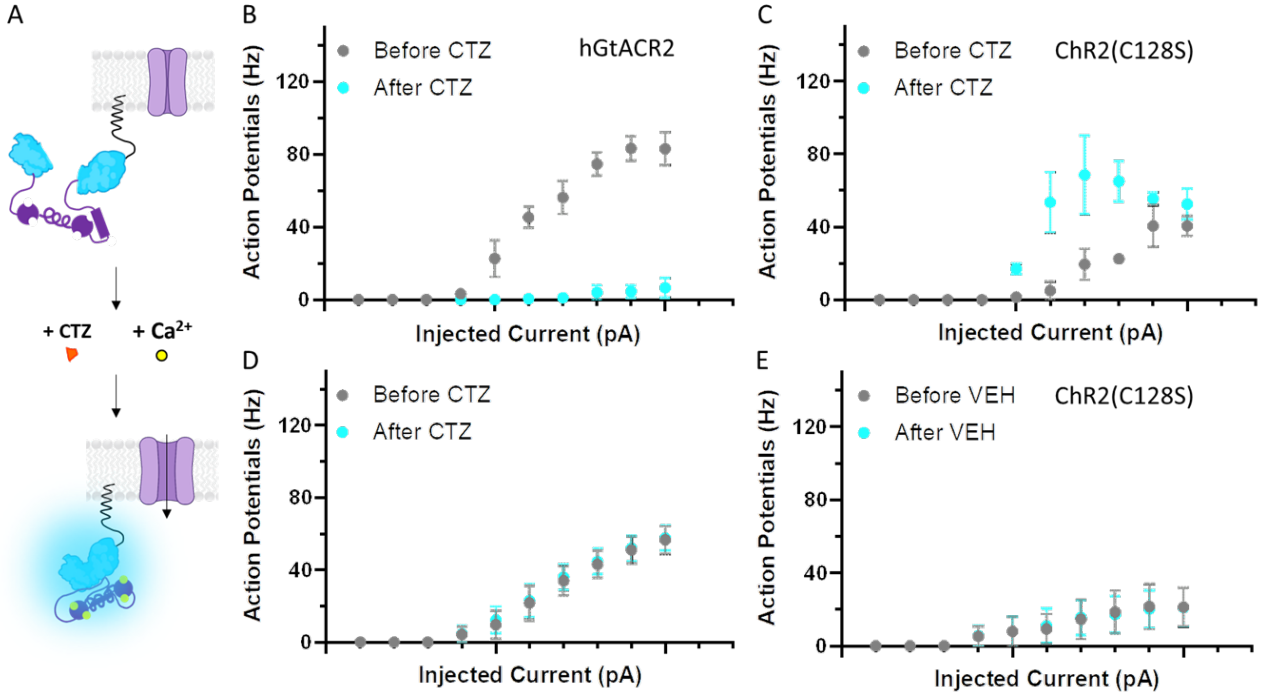
A
+ CTZ
+ Ca2+
B
hGtACR2
Before CTZ
After CTZ
Action Potentials (Hz)
Injected Current (pA)
C
ChR2(C128S)
Before CTZ
After CTZ
Action Potentials (Hz)
Injected Current (pA)
D
Before CTZ
After CTZ
Action Potentials (Hz)
Injected Current (pA)
E
ChR2(C128S)
Before VEH
After VEH
Action Potentials (Hz)
Injected Current (pA)

Figure 7

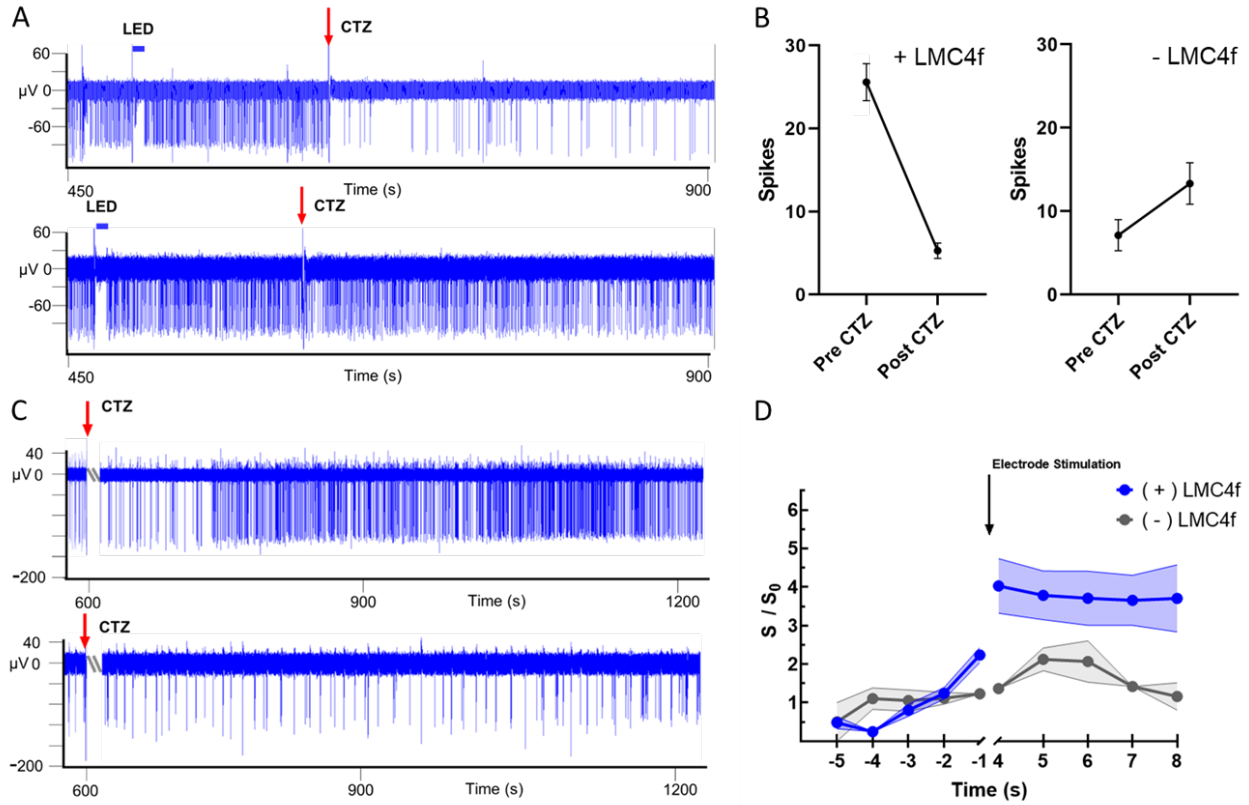
A
LED
CTZ
60
μV 0
-60
450
Time (s)
900
B
+ LMC4f
- LMC4f
Spikes
30
20
10
0
Pre CTZ
Post CTZ
C
CTZ
40
μV 0
-200
600
900
Time (s)
1200
D
Electrode Stimulation
(+) LMC4f
(-) LMC4f
S / S0
6
5
4
3
2
1
-5
-4
-3
-2
-1
4
5
6
7
8
Time (s)

Figure 8

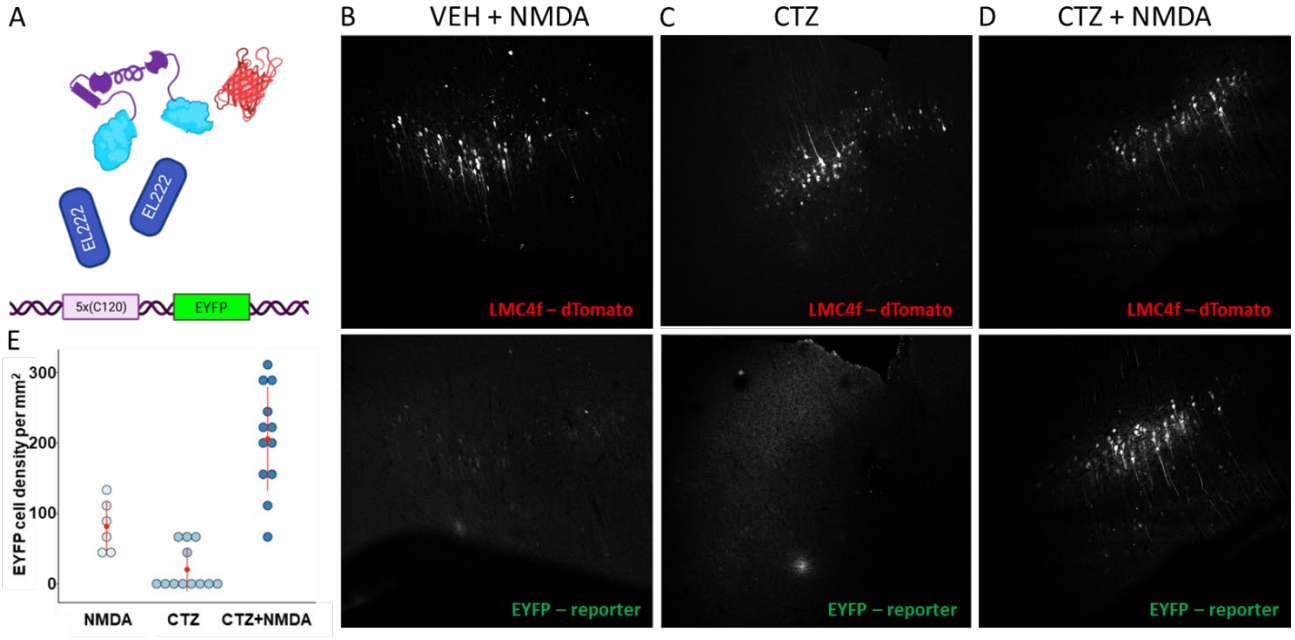
A
B
VEH + NMDA
C
CTZ
D
CTZ + NMDA
EL222
EL222
5x(C120)
EYFP
LMC4f – dTomato
LMC4f – dTomato
LMC4f – dTomato
E
EYFP cell density per mm²
300
200
100
0
NMDA
CTZ
CTZ+NMDA
EYFP – reporter
EYFP – reporter
EYFP – reporter

Figure 9

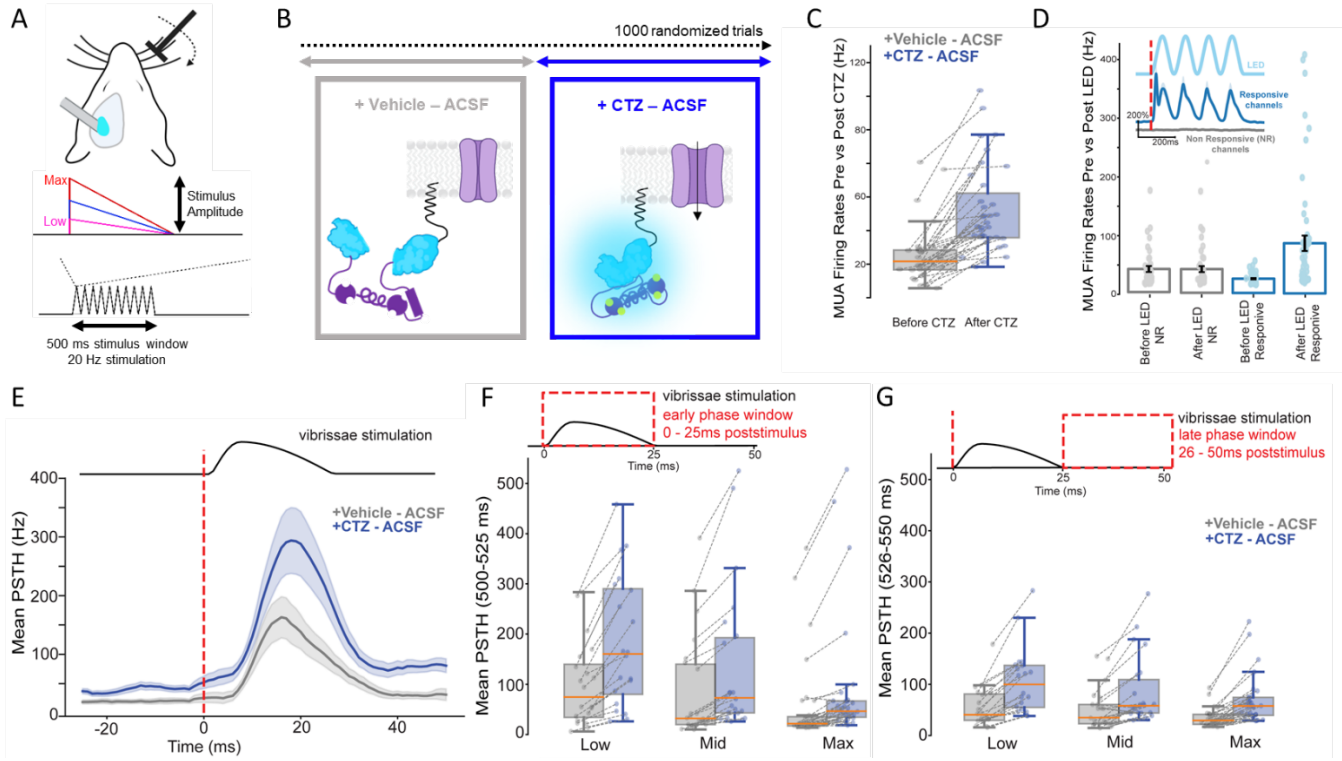
A
Max
Low
Stimulus Amplitude
500 ms stimulus window
20 Hz stimulation
B
1000 randomized trials
+ Vehicle – ACSF
+ CTZ – ACSF
C
+Vehicle - ACSF
+CTZ - ACSF
MUA Firing Rates Pre vs Post CTZ (Hz)
Before CTZ
After CTZ
D
MUA Firing Rates Pre vs Post LED (Hz)
LED
Responsive channels
Non Responsive (NR) channels
Before LED NR
After LED NR
Before LED Responive
After LED Responive
E
vibrissae stimulation
+Vehicle - ACSF
+CTZ - ACSF
Mean PSTH (Hz)
Time (ms)
F
vibrissae stimulation
early phase window
0 - 25ms poststimulus
Mean PSTH (500-525 ms)
Low
Mid
Max
G
vibrissae stimulation
late phase window
26 - 50ms poststimulus
Mean PSTH (526-550 ms)
+Vehicle - ACSF
+CTZ - ACSF
Low
Mid
Max

Supplemental Figure S1

A

sbGluc(M43L_M110L):

K[1]PTENNEDFNIVAVASNFATTDLDADRGKLPGKKLPLEVLKELEANARKAGCTRGCLIC
LSHIKC[65]TPKMKKFIPGRC[77]HTYEGDKESAQ[88]G[89]GIGEAIVDIPEIPGFKDLEPLEQF
IAQVDLCVDCTTGCLKGLANVQCSDLLKKWLPQRCATFASKIQGQVDKIKGAGGD[168]

B

LMC4: Signal Sequence; Gluc N half; CaM-M13; Gluc C half; Alpha Helix; Linker

**MGVKVLFALICIAVAEAK[1]PTENNEDFNIVAVASNFATTDLDADRGKLPGKKLPLEVLKELE
ANARKAGCTRGCLICLSHIKC[65]TPKMKKFIPGRC[77]HTYEGDKESAQ[88]GGGGTMADQLTEE
QIAEFKEEFSLFDKDGDGTITTKELGTVMRSLGQNPTEAELQDMINEVDADGDGTIDFPEF
LTMMARKMKYRDTEEEIREAFGVFDKDGNGYISAAELRHVMTNLGEKLTDEEVDEMIREAD
IDGDGQVNYEEFVQMMTAKGGKRRWKKNFIAVSAANRFKKISSSGALGSGGGG[89]GIGEAIV
DIPEIPGFKDLEPLEQFIAQVDLCVDCTTGCLKGLANVQCSDLLKKWLPQRCATFASKIQG
QVDKIKGAGGD[168]**

Supplemental Figure S2

A

```
LMC Linker-CaM-M13 Comparisons

LMC4 1    GGGGTMADQLTEEQIAEFKEEFSLFDKDGDGTITTKELGTVMRSLGQNPTEAELQDMINEVDADGDGTIDFPEFLTMMAR  80
LMC5 1    GGGGTLPDQLTEEQIAEFKEAFSLFDKDGDGTITTKELGTVMRSLGQNPTEAELQDMINEVDADGDGTIDFPEFLTMMAR  80
LMC6 1    GGGGTLPDQLTEEQIAEFKEAFSLFDKDGDGTITTKELGTVMRSLGQNPTEAELQDMINEVDADGDGTIDFPEFLTMMAR  80
LMC7 1    GGGGTMHDQLTEEQIAEFKEAFSLFDKDGDGTITTKELGTVMRSLGQNPTEAELQDMINEVDADGNGTIYFPEFLTMMAR  80
LMC8 1    GGGGTMHDQLTEEQIAEFKEAFSLFDKDGDGTITTRELGTVMRSLGQNPTEAELQDMINEVDADGNGTIYFPEFLTMMAR  80

LMC4 81   KMKYRDTEEEIREAFGVFDKDGNGYISAAELRHVMTNLGEKLTDEEVDEMIREADIDGDGQVNYEEFVQMMTAKGGKRRW  160
LMC5 81   KMKYRDTEEEIREAFGVFDKDGNGYISAAELRHVMTNLGEKLTDEEVDEMIREADIDGDGQVNYEEFVQMMTAKGGKRRW  160
LMC6 81   KGSYRDTEEEIREAFGVFDKDGNGYISAAELRHVMTNLGEKLTDEEVDEMIREADIDGDGQVNYEEFVQMMTAKGGKRRW  160
LMC7 81   KMKDTDSEEEIREAFRVFDKDGNGYISAAQLRHVMTNLGEKLTDEEVDEMIREADIDGDGQVNYEEFVQMMTAKGGKRRW  160
LMC8 81   KMKDTDSEEEIREAFRVFDKDGNGYISAAQLRHVMTNLGVKLTDEEVDEMIREADIDGDGQVNYEEFEQMMTAKGGKRRW  160

LMC4 161  KKNFIAVSAANRFKKISSSGALGSGGG  187
LMC5 161  KKNFIAVSAANRFKKISSSGALGSGGG  187
LMC6 161  KKNFIAVSAANRFKKISSSGALGSGGG  187
LMC7 161  KKNFIAVSAANRFKKISSSGALGSGGG  187
LMC8 161  KKNFIAVSAANRFKKISSSGALGSGGG  187
```

B

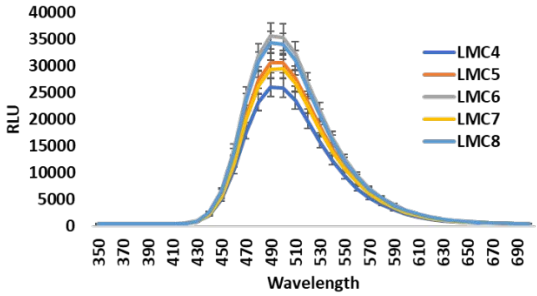

C

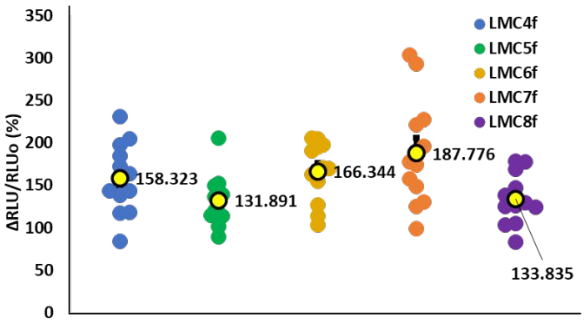
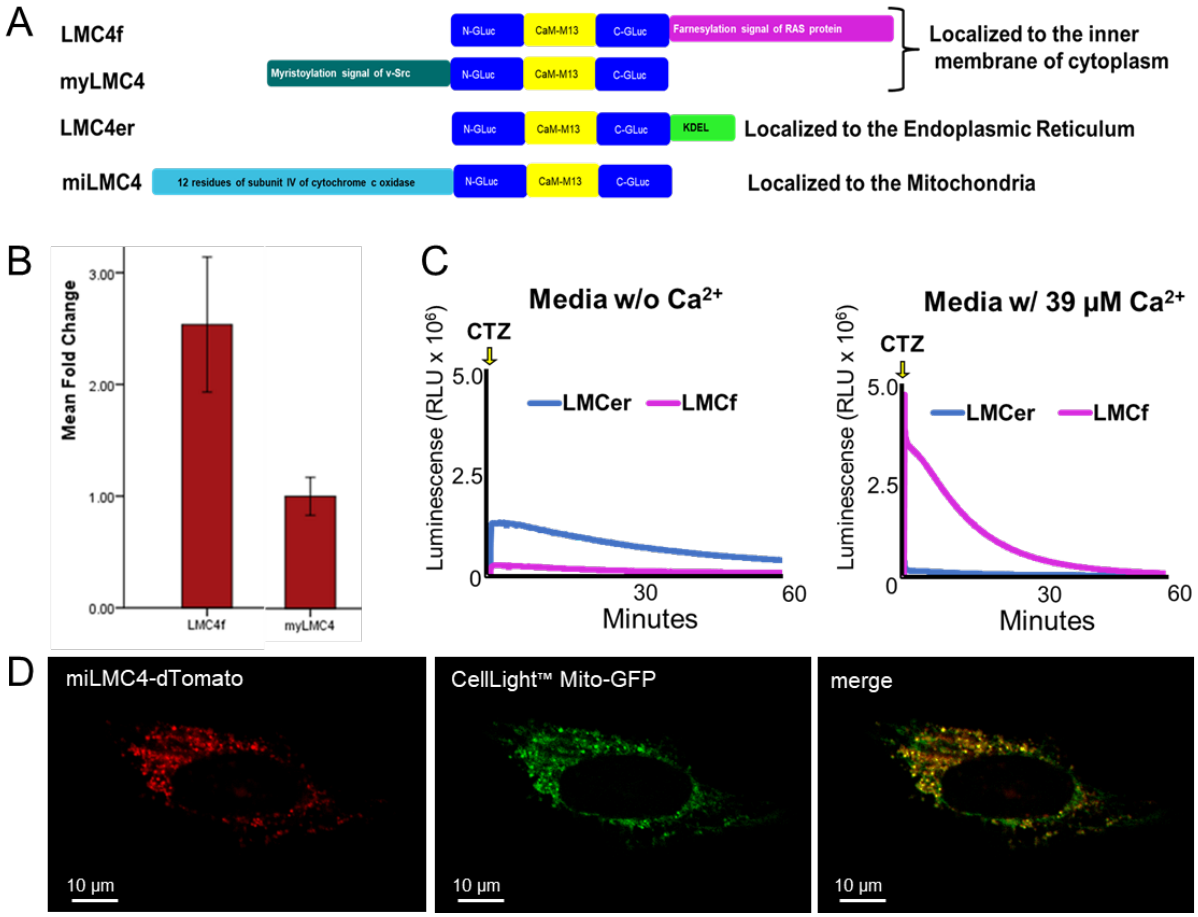
Supplemental Figure S3